The Astronomical Journal, 157:53 (14pp), 2019 February https://doi.org/10.3847/1538-3881/aaf56c
© 2019. The American Astronomical Society. All rights reserved.

Two Circumstellar Nebulae Discovered with the *Wide-field Infrared Survey Explore* and Their Massive Central Stars

Vasilii V. Gvaramadze[1,2,3], Alexei Yu. Kniazev[1,4,5], Norberto Castro[6], and Eva K. Grebel[7]
[1] Sternberg Astronomical Institute, M.V. Lomonosov Moscow State University, Universitetsky pr., 13, Moscow 119991, Russia; vgvaram@mx.iki.rssi.ru
[2] Space Research Institute, Russian Academy of Sciences, Profsoyuznaya 84/32, 117997 Moscow, Russia
[3] Isaac Newton Institute of Chile, Moscow Branch, Universitetskij Pr. 13, Moscow 119992, Russia
[4] South African Astronomical Observatory, P.O. Box 9, 7935 Observatory, Cape Town, South Africa
[5] Southern African Large Telescope Foundation, P.O. Box 9, 7935 Observatory, Cape Town, South Africa
[6] Department of Astronomy, University of Michigan, 1085 S. University Avenue, Ann Arbor, MI 48109-1107, USA
[7] Astronomisches Rechen-Institut, Zentrum für Astronomie der Universität Heidelberg, Mönchhofstr. 12-14, D-69120, Germany
Received 2018 July 31; revised 2018 November 30; accepted 2018 November 30; published 2019 January 18

Abstract

We report the discovery of two mid-infrared nebulae in the northern hemisphere with the *Wide-field Infrared Survey Explorer* and the results of optical spectroscopy of their central stars, BD+60° 2668 (composed of two components, separated from each other by ≈3 arcsec) and ALS 19653, with the Calar Alto 3.5 m telescope and the Southern African Large Telescope (SALT), respectively. We classify the components of BD+60° 2668 as stars of spectral types B0.5 II and B1.5 III. ALS 19653 is indicated in the SIMBAD database as a planetary nebula, while our observations show that it is a massive B0.5 Ib star, possibly in a binary system. Using the stellar atmosphere code FASTWIND, we derived fundamental parameters of the three stars as well as their surface element abundances, implying that all of them are either on the main sequence or only recently left it. This provides further evidence that massive stars can produce circumstellar nebulae while they are still relatively unevolved. We also report the detection of optical counterparts to the mid-infrared nebulae and a second, more extended optical nebula around ALS 19653, and present the results of SALT spectroscopy of both nebulae associated with this star. The possible origin of the nebulae is discussed.

Key words: circumstellar matter – stars: emission-line, Be – stars: individual (BD+60° 2668, ALS 19653) – stars: massive – supergiants

1. Introduction

Mid-infrared (IR) surveys of the inner regions of the Galactic plane and several other sites of massive star formation in the Milky Way carried out by the *Spitzer Space Telescope* led to the discovery of many dozens of nebulae reminiscent of circumstellar nebulae around evolved massive stars (Gvaramadze et al. 2010b; Mizuno et al. 2010; Wachter et al. 2010). Follow-up spectroscopic observations of the central sources of these nebulae showed that many of them are massive stars at different evolutionary stages (e.g., Gvaramadze et al. 2009, 2010b; Wachter et al. 2010; Stringfellow et al. 2012a, 2012b; Flagey et al. 2014; Kniazev & Gvaramadze 2015; Silva et al. 2017). Although *Spitzer* has covered the areas of the sky where most IR nebulae produced by massive stars are expected to reside, a significant number of yet undetected nebulae might remain to be uncovered. With the advent of the *Wide-field Infrared Survey Explorer* (*WISE*; Wright et al. 2010) and its all-sky survey, it became possible to search for mid-IR nebulae in regions not observed by *Spitzer*, which allowed us to discover several dozens of new nebulae (e.g., Gvaramadze et al. 2012).

Circumstellar nebulae around massive stars primarily originate from the copious mass loss inherent to these stars at different stages of their life. For example, the compact (parsec-scale) nebulae around Wolf-Rayet stars of late nitrogen sequence are produced in the course of interactions between the fast Wolf-Rayet wind and the slow, dense material lost during the preceding red supergiant phase (e.g., Brighenti & D'Ercole 1995; Garcia-Segura et al. 1996). The red supergiants themselves can also produce compact circumstellar nebulae, provided that their wind is confined by some external factors (e.g., Morris & Jura 1983; Mackey et al. 2014). Most often, circumstellar nebulae are found around (candidate) luminous blue variables (LBVs; Nota et al. 1995; Clark et al. 2005), and it is believed that they are produced by either instantaneous mass ejections or by brief (maybe recurrent) episodes of enhanced mass loss (Humphreys & Davidson 1994). Currently, more than 70% of stars of this type are known to be associated with nebulae of various shapes (Kniazev et al. 2015).

The bipolar morphology of some nebulae associated with massive stars suggests that their formation is somehow related to the (nearly critical) rotation of their underlying stars (Langer 1998). The high rotational velocity of massive stars could be intrinsic to some of them from birth or could be achieved over the course of stellar evolution, e.g., because of the contraction of a single star during the transition from core-H to core-He burning, or because of mass transfer in a close binary system. Since the majority of massive stars form in binary or multiple systems (e.g., Chini et al. 2012; Sana et al. 2012), binarity may actually be the most important factor responsible for originating circumstellar nebulae. Indeed, the presence of a second star may not only spin up its companion, but it may also trigger various modes of mass loss from the system, as has been proposed to explain the variety of shapes of planetary nebulae (e.g., Morris 1981; Fabian & Hansen 1979; Livio et al. 1979; Corradi & Schwarz 1993; Mastrodemos & Morris 1999; De Marco 2009). Moreover, a significant fraction of massive stars are already subject to binary-interaction processes (including mergers) during the main-sequence stage (Sana et al. 2012; de Mink et al. 2014), implying that circumstellar nebulae could be produced by relatively unevolved stars.

The stellar material ejected in the course of binary interaction, e.g., during the common-envelope evolution or merger of the binary components, is expected to be concentrated close to the orbital plane of the system. The resulting flattened (disk-like) circumstellar structure can, in principle, collimate the fast wind of the post-interaction binary or the merger product of two stars in the polar directions. A strong magnetic field generated during the common-envelope stage (Regös & Tout 1995; Tout & Regós 2003) or a merger of the binary components (Langer 2012; Wickramasinghe et al. 2014) could affect the geometry of the resulting circumstellar nebulae as well (see Chevalier & Luo 1994; Różyczka & Franco 1996; Garcia-Segura et al. 1999; Nordhaus & Blackman 2006).

Another potentially important mechanism for the origin of circumstellar nebulae around single (or apparently single) massive stars is connected to the bi-stability jump (Pauldrach & Puls 1990; Lamers & Pauldrach 1991)—an abrupt (a factor of 10) increase in the wind mass-loss rate (Vink 2018), $\dot{M}$, when the stellar effective temperature, $T_{\rm eff}$, decreases below the critical value of $\sim$21 kK (Lamers et al. 1995), which corresponds to a spectral type of around B1. The increase in $\dot{M}$ is accompanied (Lamers et al. 1995) by a factor of 2 decrease in the terminal wind velocity, v_{∞}, leading to a factor of $\sim$20 increase in the density of the stellar wind. In fast-rotating stars, the bi-stability jump may occur preferentially at low stellar latitudes because of the effect of gravity-darkening, which could result in an equatorial outflow (Lamers & Pauldrach 1991; Lamers et al. 1995).

Lamers et al. (2001) analyzed the chemical composition of nebulae around several LBVs and came to the conclusion that they were ejected soon after their central stars left the main sequence and that the observed chemical enhancements are due to rotationally induced mixing during the main-sequence stage. Subsequent studies of blue supergiants with LBV-like circumstellar nebulae (Smartt et al. 2002; Hendry et al. 2008; Smith et al. 2013; Gvaramadze et al. 2014, 2015, 2018; Mahy et al. 2016) lent further support to the idea that massive stars can form circumstellar nebulae during the early phases of their evolution. Two more such stars are presented in this paper.

In Section 2, we show multiwavelength images of two nebulae discovered with *WISE* and review the existing information on their central stars. Section 3 describes our optical spectroscopic observations (preliminary results of these observations were reported in Gvaramadze & Kniazev 2017). The spectral analysis of the stars is given in Section 4. In Section 5, we present and discuss spectra of an optical counterpart to one of the mid-IR nebulae. Our results are discussed in Section 6 and summarized in Section 7.

2. Two *WISE* Nebulae and Their Central Stars

In a search for rare types of massive stars through the detection of their circumstellar nebulae with *WISE*, we discovered several dozens of nebulae in regions not covered by *Spitzer*. Two of them, named WS3 and WS29 (where WS stands for "*WISE* shell"; see Gvaramadze et al. 2012), are presented below. These nebulae positionally coincide with the *Infrared Astronomical Satellite* (*IRAS*) sources IRAS 00033 +6035 and IRAS 18454+0250, respectively. The latter source is indicated in the SIMBAD database[8] as a planetary nebula. For both nebulae, we found optical counterparts in the Isaac Newton Telescope (INT) Photometric Hα Survey of the Northern Galactic Plane (IPHAS; Drew et al. 2005), which are indicated as circumstellar matter in the Hong Kong/AAO/Strasbourg Hα (HASH) planetary nebula database (Parker et al. 2016; see also Kronberger et al. 2016), and named there as PNG 117.4−01.5 (or Pa 58) and PNG 035.1+02.0, respectively. WS29 is also discernible in the Digitized Sky Survey II (DSS-II; McLean et al. 2000) red-band image and is a known source of radio emission (Condon et al. 1999). Figures 1 and 2 present *WISE* 22 and 12 μm, Two Micron All Sky Survey (2MASS; Skrutskie et al. 2006) $K_{\rm s}$-band and IPHAS Hα images of the regions containing WS3 and WS29. Figure 2 also gives the DSS-II and 1.4 GHz National Radio Astronomy Observatory (NRAO) Very Large Array (VLA) Sky Survey (NVSS; Condon et al. 1998) images of WS29.

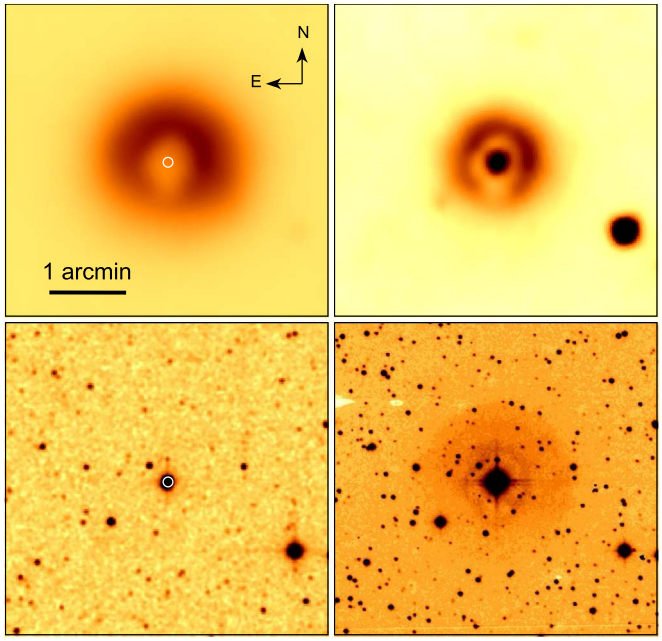

Figure 1. From left to right, and from top to bottom: *WISE* 22 and 12 μm, 2MASS $K_{\rm s}$-band, and IPHAS Hα images of the region containing BD+60° 2668 (indicated by a circle) and its circumstellar shell WS3. The orientation and the scale of the images are the same in all panels. At a distance of 3.6 kpc, 1 arcmin corresponds to $\approx$1 pc. Note the presence of two sets of (horizontal) diffraction spikes in the IPHAS image, indicating that BD+60° 2668 is composed of two components separated by $\approx$3 arcsec (see the text for details).

Figure 1 shows that WS3 is visible in both *WISE* images: at 22 μm, it appears as a thick, diffuse, almost circular shell with a radius of $\approx$1 arcmin, while at 12 μm, it appears as a slightly elongated shell with a smaller radius of $\approx$35 arcsec and a point-like source in the center. In both images, the brightness of the shell is reduced to the south. In the IPHAS Hα image, WS3 appears as a slightly elongated shell (of similar angular size to the 12 μm shell) immersed in a diffuse halo of the same extent as the emission at 22 μm. The brightness of the halo also decreases to the south, while the inner shell appears to be more extended in this direction. The observed brightness asymmetry might be caused by a density gradient in the local interstellar medium or by the motion of the local medium or the nebula itself.

Using the SIMBAD database, we identified the central source of WS3 as the optical star BD+60° 2668, which is known as a double or multiple system (Douglass et al. 1999). A literature search revealed that BD+60°2668 was recognized as

[8] http://simbad.harvard.edu/simbad/

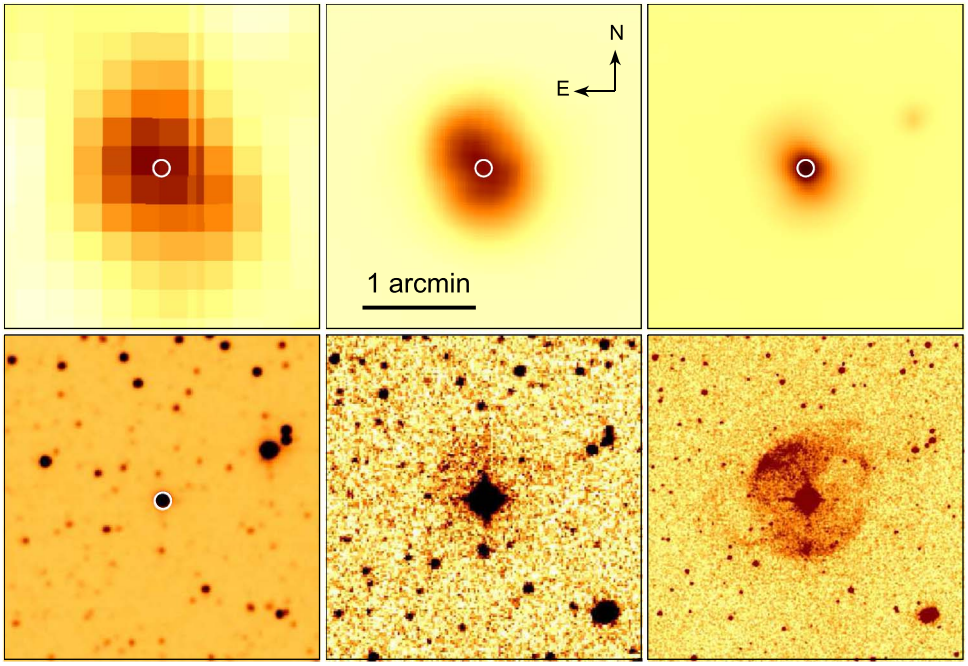

Figure 2. From left to right, and from top to bottom: NVSS 1.4 GHz, *WISE* 22 and 12 μm, 2MASS K_s-band, DSS-II red-band, and IPHAS Hα images of the region containing ALS 19653 (indicated by a circle) and its circumstellar shell WS29. The orientation and the scale of the images are the same in all panels. At a distance of 1.57 kpc, 1 arcmin corresponds to ≈0.45 pc.

an OB star by Nassau & Morgan (1951) and classified as B2 by Brodskaya (1953), as B1 III by Morgan et al. (1955), and more recently as B1 by Radoslavova (1989). According to Douglass et al. (1999), BD+60°2668 is composed of two stars, hereafter BD+60°2668A and BD+60°2668B, separated from each other by ≈3 arcsec, and lying on a line with a position angle (PA) of ≈159° (measured from north to east). The second data release of *Gaia* (DR2; Gaia Collaboration et al. 2018) provides for BD +60° 2668A and BD+60° 2668B accurate parallaxes of 0.2827 ± 0.0290 mas and 0.2643 ± 0.0347 mas, placing these stars at $d = 3.54^{+0.40}_{-0.33}$ kpc and $3.78^{+0.57}_{-0.44}$ kpc, respectively. In what follows, we adopt a distance of 3.6 kpc to both stars as well as to WS3 (see Section 6.1). At this distance, 1 arcmin corresponds to ≈1 pc. Some of the properties of BD+60° 2668A and BD+60°2668B are summarized in Table 1.

The IR morphology of WS29 differs completely from that of WS3 (see Figure 2). At 22 μm, WS29 has a dumbbell-like shape with the long axis oriented in the northeast–southwest direction (PA ≈ 30°). At 12 μm, the nebula appears as a centrally brightened source, slightly elongated in the same direction as the 22 μm nebula. In the Hα image, WS29 appears as an almost circular shell of angular diameter of about 1 arcmin with enhanced brightness on the northeast and southwest sides, i.e., in the places where the IR nebula is in apparent contact with the optical shell. This image also shows several filaments extending in the northwest and southeast directions beyond the main shell, suggesting that there are protrusions in the shell along the line perpendicular to the IR nebula (PA ≈ 120°). The IPHAS Hα image also shows that WS29 is surrounded by a more extended shell of angular radius of about 2.7 arcmin. This shell is more prominent to the east and northeast, but can also be discerned to the west and southwest of WS29 (see Figure 3 and Sections 5 and 6.2).

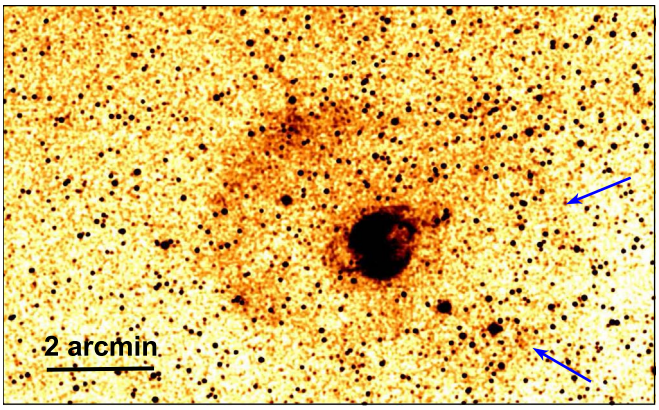

Figure 3. IPHAS Hα image of a region around WS29 showing the presence of a second, more extended shell. This shell is more prominent to the east and northeast, but can also be discerned to the west and southwest from WS29 (as indicated by arrows). North is up, east is left.

Table 1
Properties of BD+60° 2668A&B and ALS 19653

	BD+60° 2668A (WS3)	BD+60° 2668B (WS3)	ALS 19653 (WS29)
SpT	B0.5 II	B1.5 III	B0.5 Ib
α (J2000)	$00^h06^m01\overset{s}{.}39$	$00^h06^m01\overset{s}{.}52$	$18^h48^m00\overset{s}{.}66$
δ (J2000)	60°52′02″.0	60°51′59″.1	02°54′17″.1
l	$117\overset{\circ}{.}4303$	$117\overset{\circ}{.}4304$	$35\overset{\circ}{.}1279$
b	$-1\overset{\circ}{.}5185$	$-1\overset{\circ}{.}5193$	$2\overset{\circ}{.}0859$
B (mag)	9.86 ± 0.02	10.33 ± 0.03	14.40 ± 0.04
V (mag)	9.48 ± 0.02	10.00 ± 0.04	12.40 ± 0.05

Note. The spectral types are based on our spectroscopic observations. The coordinates and photometry of BD+60° 2668A&B are from Kharchenko (2001), while those of ALS 19653 are from Henden et al. (2016).

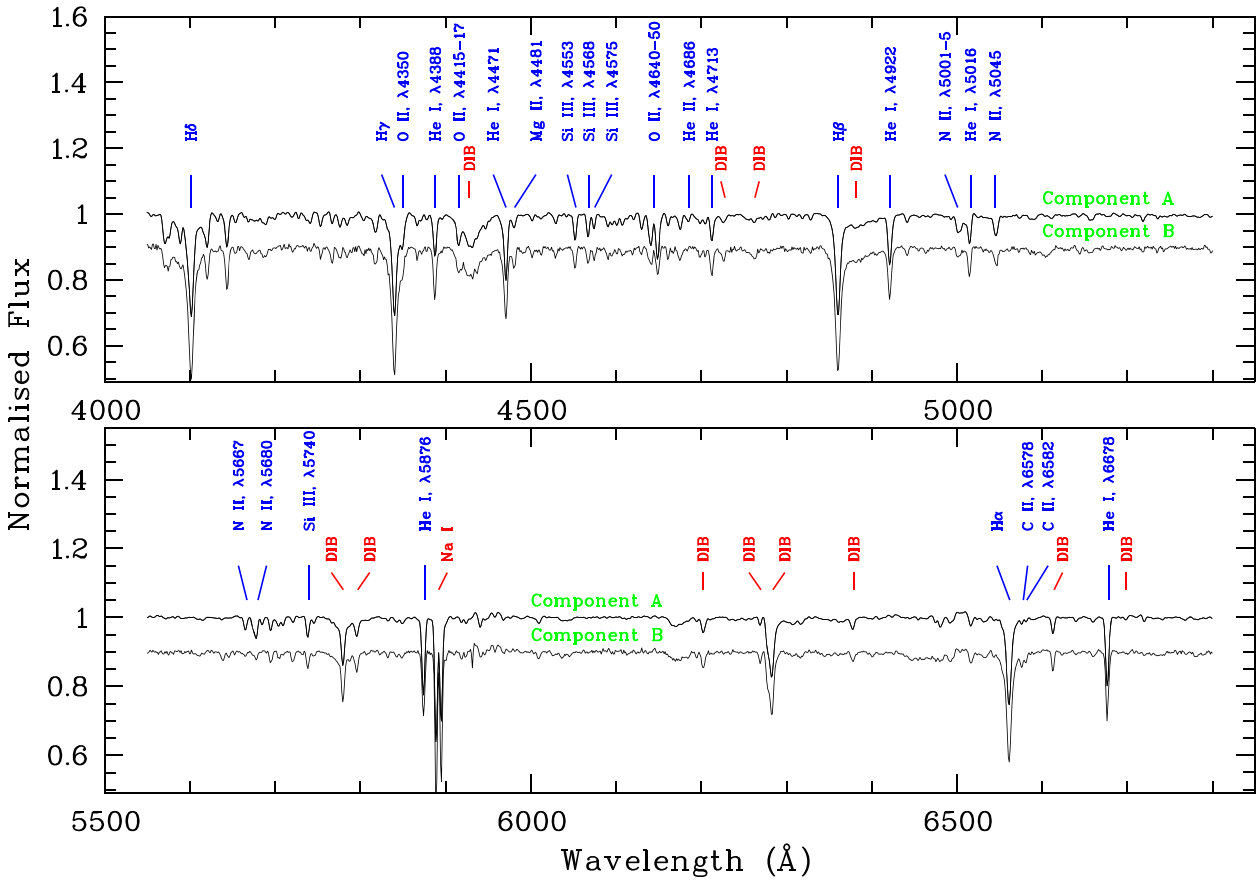

Figure 4. Normalized spectra of the two components of BD+60° 2668 obtained with the TWIN spectrograph at the 3.5 m telescope at the Calar Alto Observatory. The principal lines and most prominent diffuse interstellar bands (DIBs) are indicated.

Using the SIMBAD database, we found that the central star of WS29, known as ALS 19653 (or PDS 543), was classified as a B1 star by Vieira et al. (2003). Condon et al. (1999) detected an elongated radio source at the position of WS29 in the 1.4 GHz NVSS image (see Figure 2) with major and minor axes of ≈77 and 47 arcsec, respectively. The PA of the major axis of ≈24° is similar to that of the *WISE* 22 μm nebula. Moreover, polarimetric observations of ALS 19653 by Rodrigues et al. (2009) revealed an intrinsic polarization of the star of 1.14% ± 0.04% with a polarization angle of 121°. This implies the presence of a non-spherical structure around the star with the major axis at PA ≈ 30° (i.e., parallel to the major axis of the 22 μm nebula). The *Gaia* DR2 parallax of ALS 19653 of 0.6388 ± 0.0633 mas (Gaia Collaboration et al. 2018) places this star at $d = 1.57^{+0.17}_{-0.14}$ kpc. At a distance of 1.57 kpc, 1 arcmin corresponds to ≈0.45 pc. Some of the properties of ALS 19653 are summarized in Table 1. Note that ALS 19653 is much more reddened compared to BD+60° 2668A&B ($B - V = 2$ mag versus $B - V \approx 0.3$ mag) despite having a factor of 2 shorter distance to the former star.

3. Spectroscopic Observations

3.1. BD+60° 2668A&B

Spectra of BD+60° 2668A&B were obtained with the TWIN spectrograph attached to the Cassegrain focus of the 3.5 m telescope in the Observatory of Calar Alto (Spain) on 2012 July 12. Three exposures of 60 s were taken. The setup used for TWIN consisted of the gratings T08 in the first order for the blue arm (spectral range of 3500–5600 Å) and T04 in the first order for the red arm (spectral range of 5300–7600 Å), providing a reciprocal dispersion of 72 Å mm^{-1} for both arms. The resulting FWHM spectral resolution measured on strong lines of the night sky and reference spectra was 3.1–3.7 Å. The slit of 240 × 2.1 arcsec^2 was oriented at a PA selected in a way to observe both stars simultaneously. The seeing during the observations was not stable, ≃1.0–1.5 arcsec. Spectra of the He–Ar comparison arcs were obtained to calibrate the wavelength scale, and spectrophotometric standard star BD+33° 2642 (Bohlin 1996) was observed at the beginning of the night for the flux calibration.

The primary data reduction was done using the IRAF package. The data for each CCD detector were trimmed, bias-subtracted, and flat-corrected. The subsequent long-slit data reduction was carried out in the way described in Kniazev et al. (2008). The two-dimensional (2D) spectra were averaged, and one-dimensional (1D) spectra for both components were then extracted using the IRAF APALL task. The resulting normalized 1D spectra are shown in Figure 4.

Unfortunately, the optical counterpart to WS3 was discovered after the spectra of the central stars were obtained. The short total exposure used for the spectroscopy of these bright stars did not allow us to detect signatures of the nebular emission in the 2D spectrum.

3.2. ALS 19653

Spectra of ALS 19653 and the optical shells around it were taken with the Robert Stobie Spectrograph (RSS;

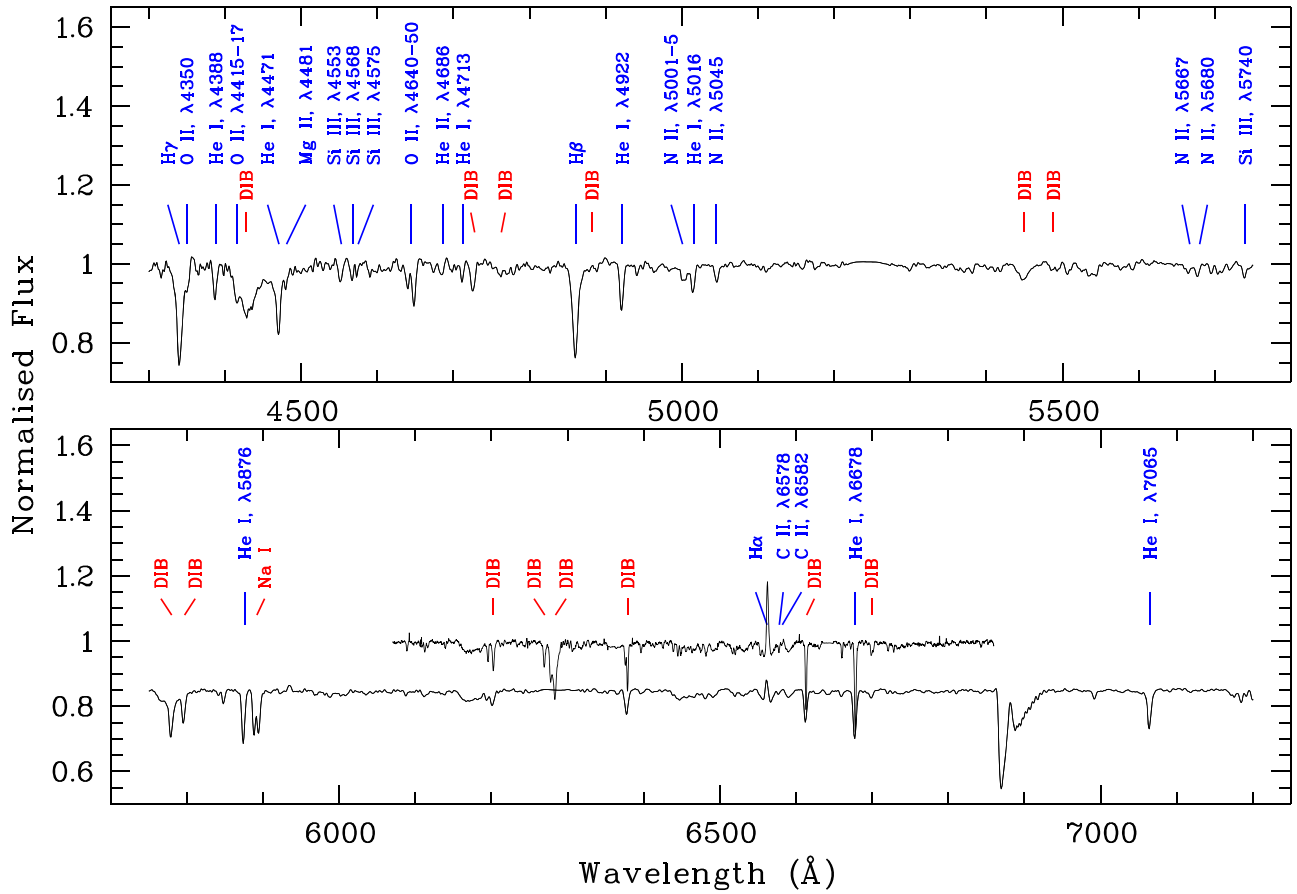

Figure 5. Normalized low-resolution RSS spectrum of ALS 19653 obtained with the SALT on 2016 April 25. The principal lines and most prominent DIBs are indicated. The lower panel also shows the high-resolution RSS spectrum (upper curve) obtained on 2016 May 28.

Table 2
Journal of SALT Observations of ALS 19653 and Its Circumstellar Nebula WS29

Instrument	Date	Exposure (s)	Spectral Scale (Å pixel^{-1})	Slit (arcsec)	PA (°)	Seeing (arcsec)	Spectral Range (Å)
RSS	2016 Apr 25	240	0.97	1.25	0	1.6	4200–7300
HRS	2016 May 27	1500	0.04	⋯	⋯	3.0	3700–8900
RSS	2016 May 28	1200	0.26	2.00	33	2.1	6035–6870
RSS	2016 Jun 17	1800	0.26	2.00	120	2.1	6035–6870
HRS	2017 Oct 5	1500	0.04	⋯	⋯	3.0	3700–8900

Burgh et al. 2003; Kobulnicky et al. 2003) mounted on the Southern African Large Telescope (SALT; Buckley et al. 2006; O'Donoghue et al. 2006). Observations were carried out in the long-slit mode on three occasions during 2016 (logged in Table 2). The PG900 grating was used for the first observation (PA = 0°) to cover the spectral range of 4200–7300 Å with a final reciprocal dispersion of 0.97 Å pixel^{-1}. The spectral resolution FWHM was 4.43 ± 0.18 Å. We call this spectrum low resolution hereafter. A Xe lamp arc spectrum was taken immediately after the science frame. Spectrophotometric standard stars were observed during twilight time for the relative flux calibration. To study the radial velocity and Hα intensity distributions in WS29 and its surroundings, we obtained two additional spectra of higher resolution with the PG2300 grating and two different orientations of the slit. The slit was placed on ALS 19653 and oriented in such a way to cross the brightest sides of the shell (PA = 33°) and the protrusions in the shell (PA = 120°). The obtained spectra cover the spectral range of 6035–6870 Å with a final reciprocal dispersion of 0.26 Å pixel^{-1} and the spectral resolution FWHM of 1.85 ± 0.11 Å. We call these spectra high resolution hereafter. A Ne lamp arc spectrum was taken immediately after the science frames. The spatial scale of all three RSS spectra was 0.51 arcsec pixel^{-1}.

Primary reduction of the RSS data was done in the standard way with the SALT science pipeline (Crawford et al. 2010). The subsequent long-slit data reduction was carried out in the way described in Kniazev et al. (2008). The resulting reduced RSS spectrum of ALS 19653 is shown in Figure 5, while that of WS29 is presented and discussed in Section 5.

To study ALS 19653 in more detail and to search for possible radial velocity variations, we observed this star with the SALT High Resolution Spectrograph (HRS; Barnes et al. 2008; Bramall et al. 2010, 2012; Crause et al. 2014) on two occasions, 2016 May 27 and 2017 October 5, with single exposures of 1500 s and a seeing of about 3 arcsec (see Table 2). The HRS is a dual-beam, fiber-fed échelle spectrograph. It was used in the

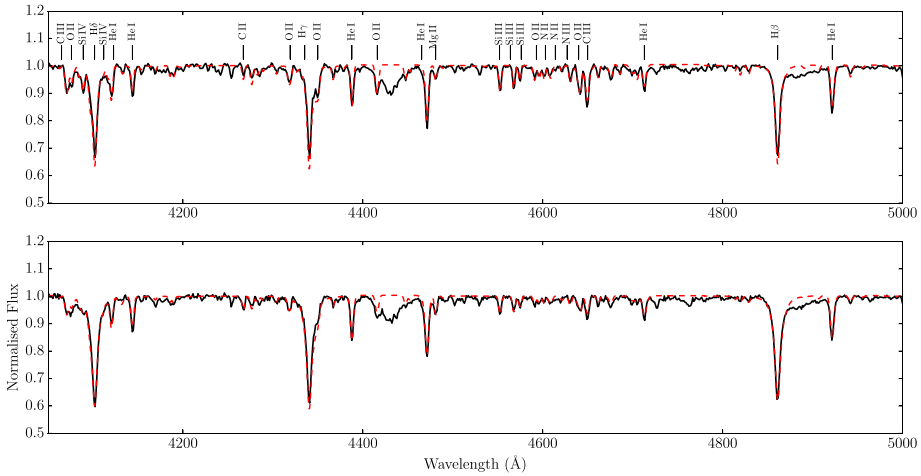

Figure 6. Parts of the normalized spectra of BD+60° 2668A and BD+60° 2668B (shown, respectively, in the upper and bottom panels by the black lines) compared with the best-fitting FASTWIND models (red dashed lines) with the parameters as given in Tables 3 and 4. The lines fitted by the models are indicated.

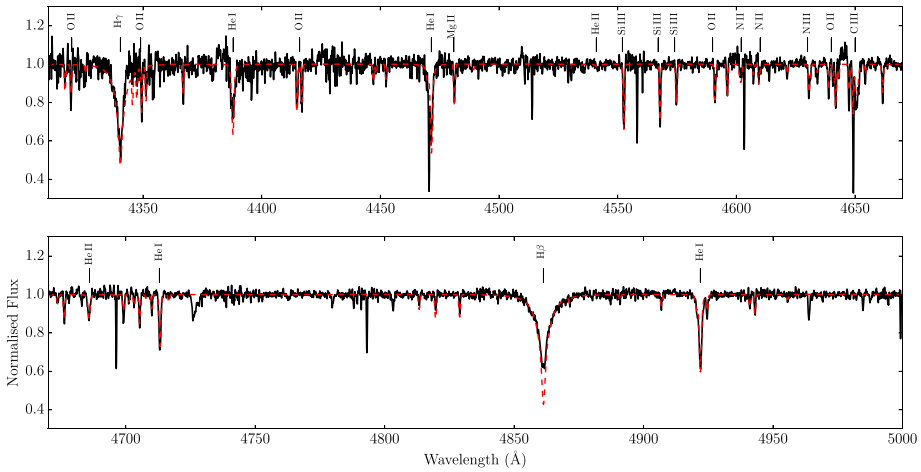

Figure 7. Parts of the normalized and rebinned SALT HRS spectrum of ALS 19653 (black line) compared with the best-fitting FASTWIND model (red dashed line) with the parameters as given in Tables 3 and 4. The lines fitted by the model are indicated.

medium-resolution mode (R = 40,000–43,000 and 2.23 arcsec diameter for both the object and sky fibers) to obtain a spectrum in the blue and red arms over the total spectral range of ≈3700–8900 Å. Both the blue and red arm CCDs were read out by a single amplifier with a 1 × 1 binning. Three arc spectra of the ThAr lamp and three spectral flats were obtained for each observation in this mode during a weekly set of HRS calibrations.

Primary reduction of the HRS spectra was performed with the SALT science pipeline (Crawford et al. 2010). The subsequent reduction steps, including background subtraction, order extraction, removal of the blaze function, identification of the arc lines, and merging of the orders for the object spectra, were carried out using the MIDAS HRS pipeline described in detail in Kniazev et al. (2016). Parts of the 2016s HRS spectrum are shown in Figure 7.

4. Spectral Analysis and Stellar Parameters

4.1. Classification of BD+60° 2668A&B and ALS 19653

The spectra of BD+60° 2668A&B and ALS 19653 are dominated by H I and He I absorption lines (see Figures 4 and 5). Two of these stars (BD+60° 2668A and ALS 19653) show the He II λ4686 line, implying that they are B stars of spectral types earlier than B0.7 (Walborn & Fitzpatrick 1990). The HRS spectrum of ALS 19653 also shows the presence of the weak He II λ4541 line. The only emission line detected is that of Hα in the spectrum of ALS 19653. We attribute this emission to the circumstellar material around the star (see the next subsection). Note the presence of a prominent diffuse interstellar band (DIB) at 6379 Å in the spectra of BD+60° 2668A&B, creating the illusion of asymmetry in the Hβ line profile (see Figures 6 and 7).

Using the classification criteria from Evans et al. (2004), we classify BD+60° 2668A and ALS 19653 as B0.5,[9] and BD+60° 2668B as B1.5. The measured equivalent widths (EWs) of the Hγ line in the spectra of BD+60° 2668A, BD +60° 2668B, and ALS 19653 of 2.06 ± 0.09, 2.90 ± 0.11, and 1.42 ± 0.04 Å, respectively, and the EW(Hγ)–absolute magnitude calibration by Balona & Crampton (1974) suggest

[9] Although the He II λ4541 line was detected in the HRS spectrum of ALS 19653, we do not take it into account because the classification criteria in Evans et al. (2004) are based on much lower resolution spectra.

Table 3
Stellar Parameters for BD+60° 2668A&B and ALS 19653

	BD+60° 2668A	BD+60° 2668B	ALS 19653
$T_{\rm eff}$ (kK)	$26.0^{+1.7}_{-1.8}$	$23.0^{+1.4}_{-1.2}$	$26.0^{+1.3}_{-1.7}$
$\log g$	$3.30^{+0.14}_{-0.15}$	$3.60^{+0.17}_{-0.12}$	$3.10^{+0.26}_{-0.28}$
ξ (km s^{-1})	9 ± 2	8 ± 2	7 ± 2
$v \sin i$ (km s^{-1})	130	150	28
$v_{\rm r,hel}$ (km s^{-1})	-20.9 ± 2.1	-20.9 ± 3.6	see Table 5

for these stars the luminosity classes of Ib, III, and Ia. The luminosity classes derived for BD+60° 2668A and ALS 19653, however, are inconsistent with the absolute visual magnitudes of these stars of $M_V \approx -5.4$ mag and -5.5 mag (see Section 6), which instead imply the luminosity classes of II and Ib, respectively (e.g., Humphreys & McElroy 1984). We therefore regard BD+60° 2668A and ALS 19653 as B0.5 II and B0.5 Ib stars.

4.2. Spectral Modeling

The stellar atmosphere analysis of the three stars is rooted on a large grid of synthetic stellar atmosphere models built using the atmosphere/line formation code FASTWIND (Santolaya-Rey et al. 1997; Puls et al. 2005; Rivero González et al. 2012). The FASTWIND stellar code takes into account non-local thermodynamic equilibrium effects in spherical symmetry with an explicit treatment of the stellar wind. The stellar grid was designed to accomplish the analysis of late O- and B-type stars with an effective temperature, $T_{\rm eff}$, between 34,000 and 12,000 K in 1000 K steps, and a surface gravity, $\log g$, between 4.4 and 2.0 dex in steps of 0.1 dex. The helium abundance was fixed at the solar value. Explicit atomic models for H I; He I,II; N II,III; O II,III; C II,III; Si II,III,IV; and Mg II were included in the determination of the fundamental stellar parameters and chemical abundances. The rest of the chemical species were treated in an implicit way to account for blanketing/blocking effects. For further details, see Puls et al. (2005).

First, several key lines in the spectra[10] were simultaneously compared with the grid looking for the set of stellar parameters that best reproduces the spectrum, following the routines and the line list described in Castro et al. (2012; see also Lefever et al. 2010). Subsequently, and based on the best predicted effective temperatures and gravities, new synthetic subgrids were built for each star with chemical abundances varying around the cosmic abundance standard (CAS) in the solar neighborhood (Nieva & Przybilla 2012) in steps of 0.2 dex and microturbulence velocities, ξ, spanning from 1 to 15 km s^{-1} in steps of 1 km s^{-1}. The best combination of abundances and microturbulence that reproduces the observations were found through an optimized genetic algorithm. The main chemical transitions modeled in this study are labeled in Figures 6 and 7 (see also Table 4 in Castro et al. 2012). The derived stellar parameters and chemical abundances are listed in Tables 3 and 4.

The high resolution of the HRS spectrum of ALS 19653 allowed us to determine the projected rotational velocity, $v \sin i$, through the Fourier transform of the Si III λ4552 line profile using the IACOB-BROAD code (Simón-Diaz & Herrero 2007, 2014). The much lower spectral resolution of the TWIN spectra prevents us from applying the same technique for BD +60° 2668A&B. For these stars, after a first guess of the best stellar parameters, we convolved the synthetic spectra until we reproduced the FWHM of the metallic lines. This procedure was repeated, updating $v \sin i$ until it converged and we reached the best combination of stellar parameters and $v \sin i$ that fits the observations. The obtained values of $v \sin i$ are given in Table 3. We note that the actual values of $v \sin i$ derived for BD +60° 2668A&B could be smaller because the measured velocities are around the limit imposed by the low spectral resolution.

We also estimated the heliocentric radial velocities, $v_{\rm r,hel}$, of all three stars using the ULYSS (University of Lyon Spectroscopic analysis Software) program (Koleva et al. 2009) with a medium spectral resolution library (Prugniel et al. 2011). For BD+60° 2668A&B, we derived almost equal velocities (see Table 3). For ALS 19653, we used all five RSS and HRS spectra and found significant radial velocity variations ($\Delta v_{\rm r,hel} \approx 50$ km s^{-1}; see Table 5). These changes suggest that ALS 19653 is a close binary system, which was in the periastron passage between 2016 April 25 and May 27.

To get an idea of the possible parameters of the binary system, we assume that its orbit is circular and fit the data points to a sine curve using the χ^2 algorithm. The best-fitting result ($\chi^2 = 2.33 \times 10^{-3}$) is shown in Figure 8 and implies an orbital period of 164.20 ± 0.02 days, an amplitude of 33.33 ± 0.04 km s^{-1}, and a systemic velocity of -9.02 ± 0.05 km s^{-1}. We realize that this solution is not unique because of the limited number of data points. Time-series spectroscopy and photometry of ALS 19653 are required to determine the actual parameters of the system.

Still, using the above parameters of the binary and the mass of ALS 19653 of $\approx 20\,M\odot$ (see Section 6.2), one can estimate the mass of the companion star to be $\approx 8\,M\odot$. Assuming that this star is on the main sequence, one finds that its V-band brightness should be a factor of ~20–30 lower than that of ALS 19653. This is consistent with the non-detection of double-lined structures in the HRS spectra of ALS 19653, although both spectra were obtained at the time favorable for their detection, i.e., when the difference in the radial velocities of the binary components was close to maximum (see Figure 8 and Table 5).

The presence of the Hα emission line in the spectrum of ALS 19653 (see Figure 5) could indicate that this star possesses a strong wind. In Figure 9, we compare the observed Hα line profile (from the HRS spectrum obtained on 2016 May 27) with synthetic ones obtained in FASTWIND models with four different mass-loss rates. In these models, we adopted a wind velocity law exponent $\beta = 2$ and a terminal wind velocity of 1500 km s^{-1}, based on the effective temperature of ALS 19653 and the empirical calibration in Kudritzki & Puls (2000). The intensity of the observed line matches a mass-loss rate of $\approx 4 \times 10^{-7}\,M\odot$ yr^{-1}. However, the synthetic lines have a P-Cygni-type profile (typical of lines formed in powerful winds or expanding gaseous shells), while in the observed line, the intensity peak is shifted to the violet side with respect to the peaks of the model lines, and the line itself has an asymmetric shape with an absorption dip on the red side (see also Figure 10). This suggests that the Hα emission is instead formed in the circumstellar material around the star.

The circumstellar origin of the Hα line is also suggested by changes in the profile of this line. Figure 10 shows that in 2016,

[10] For the spectral modeling of ALS 19653, we used the HRS spectrum obtained on 2016 May 25.

Table 4
Elemental Abundances (by Number) in BD+60° 2668A&B and ALS 19653

	BD+60° 2668A	BD+60° 2668B	ALS 19653	CAS	Brott et al. (2011)
log(C/H)+12	$7.7^{+0.2}_{-0.2}$	$7.5^{+0.2}_{-0.2}$	$7.9^{+0.5}_{-0.2}$	8.33 ± 0.04	8.13
log(N/H)+12	$8.3^{+0.2}_{-0.2}$	$7.9^{+0.1}_{-0.2}$	$7.9^{+0.2}_{-0.2}$	7.79 ± 0.04	7.64
log(O/H)+12	$8.7^{+0.1}_{-0.1}$	$8.8^{+0.1}_{-0.1}$	$8.5^{+0.2}_{-0.2}$	8.76 ± 0.05	8.55
log(Mg/H)+12	$7.6^{+0.4}_{-0.5}$	$7.7^{+0.4}_{-0.2}$	$7.5^{+0.3}_{-0.1}$	7.50 ± 0.05	7.32
log(Si/H)+12	$7.6^{+0.2}_{-0.3}$	$7.5^{+0.2}_{-0.1}$	$7.5^{+0.2}_{-0.1}$	7.56 ± 0.05	7.41

Note. The cosmic abundance standard (CAS; Nieva & Przybilla 2012) in the solar neighborhood and initial abundances adopted in the evolutionary models by Brott et al. (2011) are given for reference. Note the enhanced nitrogen abundance in BD+60° 2668A.

Table 5
Heliocentric Radial Velocity Changes with Time in the Spectrum of ALS 19653

Date	$v_{r,hel}$ (km s^{-1})	Spectrograph
2016 Apr 5	−29 ± 3	RSS GR900
2016 May 27	+9.25 ± 0.33	HRS
2016 May 28	+10.2 ± 0.5	RSS GR2300
2016 Jun 17	+23.7 ± 1.3	RSS GR2300
2017 Oct 5	+12.18 ± 1.33	HRS

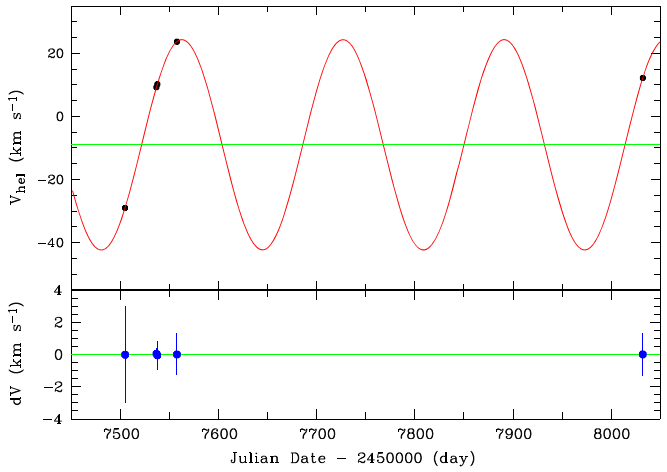

Figure 8. Radial velocity changes with time in the spectrum of ALS 19653.

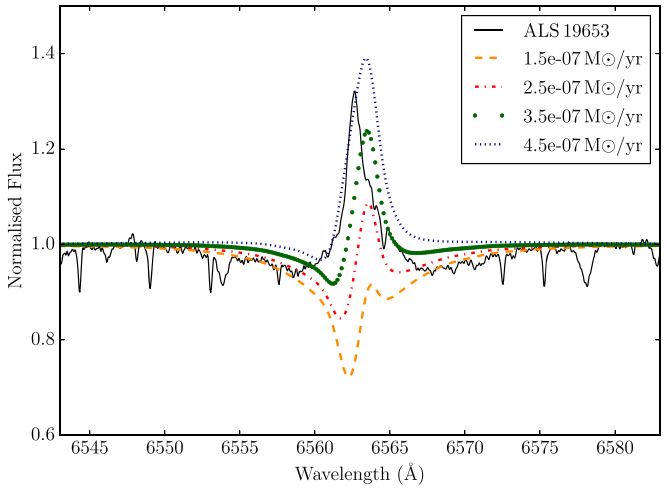

Figure 9. Comparison of the observed profile of the Hα line with synthetic profiles predicted by FASTWIND models with different values of the mass-loss rate as specified in the legend.

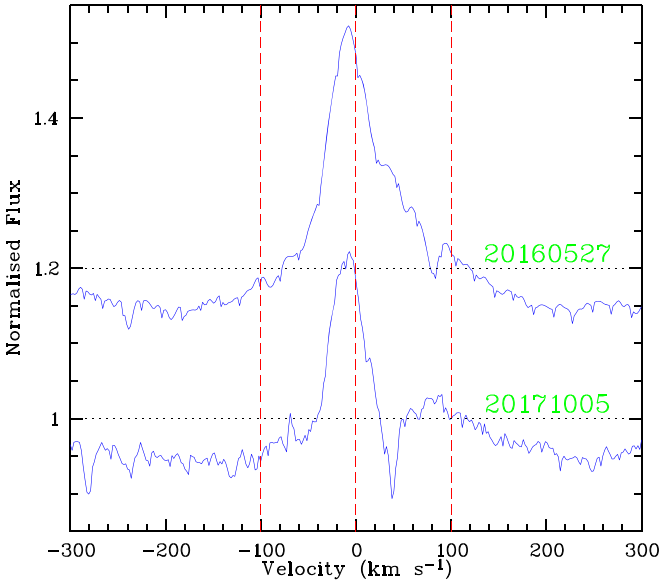

Figure 10. Changes in the Hα line profile in the HRS spectra of ALS 19653. The upper line profile corresponds to the spectrum from 2016 May 27, while the lower one to the spectrum from 2017 October 5.

the Hα line was dominated by a sharp asymmetric emission and also shows the presence of a second, much weaker emission component at ≈90 km s^{-1}, separated from the first one by a shallow absorption dip at ≈80 km s^{-1}. In 2017, the two-peak shape of the Hα line became more obvious after the absorption dip had extended below the continuum and shifted bluewards to ≈40 km s^{-1}. This change in the absorption was accompanied by a ≈10% decrease of the intensity of the main emission component and a blueward shift of the second emission peak. A similar behavior of the Hα emission line was detected in late-B and early-A supergiants (e.g., Kaufer et al. 1996; Markova & Valchev 2000; Verdugo et al. 2000), where the shape of this line changes from blue- or redshifted asymmetric emission to a double-peaked or inverse P Cygni profile (see, e.g., Figure 1 in Markova & Valchev 2000 for a good example of these changes). This behavior of the line profile was interpreted in terms of the deviation of the stellar wind from spherical symmetry or the presence of a flattened (disk-like) circumstellar structure (e.g., Kaufer et al. 1996; Petrenz & Puls 1996; Fullerton et al. 1997). The presence of an elongated (IR) nebula around ALS 19653 and the detection of intrinsic polarization of this star (with the polarization angle aligned with the elongated nebula) make it natural to assume that the Hα line originates in a flattened circumstellar structure (viewed nearly edge-on) and that its variability is caused by a

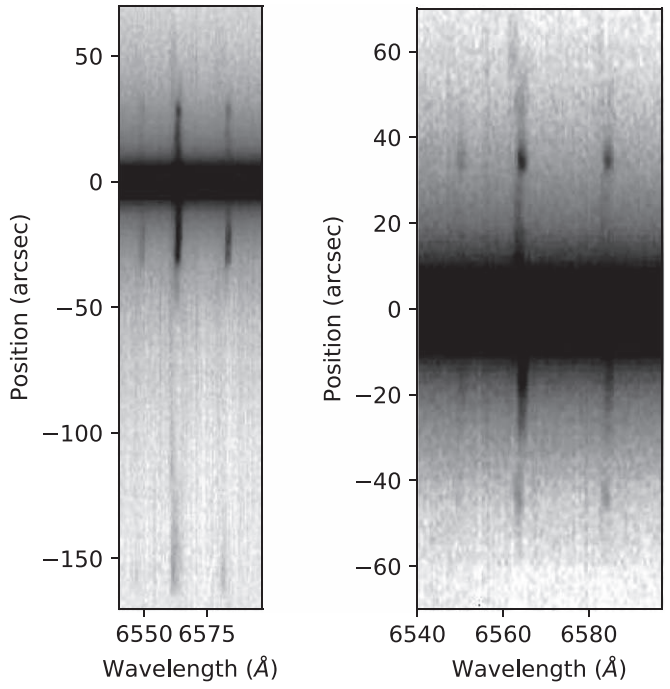

Figure 11. Portions of the 2D high-resolution RSS spectra of WS29, showing the Hα and [N II] $\lambda\lambda$6548, 6584 lines. The left- and right-hand panels correspond, respectively, to the slit orientation of PA = 33° and 120°. Negative offsets in the left-hand panel correspond to the northeast side of the slit, while those in the right-hand panel to the southeast side of the slit.

large-scale density asymmetry in this structure (see Section 6.2).

5. Spectroscopy of WS29

As noted in Section 3, we obtained two high-resolution RSS spectra of WS29 with the slit placed on ALS 19653 and oriented at PA = 33° and 120°. The 8 arcmin long slit allowed us also to obtain spectra of the second, more extended shell around ALS 19653 (see Figure 3). The only lines detected in the spectra of WS29 and the second shell are those of Hα and [N II] $\lambda\lambda$6548, 6584. Portions of the 2D spectra showing these lines are presented in Figure 11. The left-hand panel shows that the second shell extends in the northeast direction for ≈160 arcsec from the star and that the emission lines from the shell are split into two components, indicating expansion of the shell. The splitting of the emission lines is also visible in the right-hand panel (at about 60 arcsec southwest of the star), indicating the presence of material with different radial velocities (see Figure 12).

Using the 2D spectra, we plot the distributions of the Hα and [N II] λ6584 emission line intensities and the Hα heliocentric radial velocity, $V_{\rm hel}$, along the slits (see the upper panels in Figure 12, where the left- and right-hand panels correspond, respectively, to the slit orientations of PA = 120° and 33°). The plots show that the intensities of both lines correlate with bright details in WS29 and the second shell. In particular, the plots also show that WS29 is more extended in the southeast–northwest direction (PA = 120°) than in the orthogonal direction.

The position–velocity diagram obtained for the slit with PA = 33° shows that the nearby side of the second shell approaches us with a velocity of ∼100 km s^{-1}. The velocity field in WS29 is more complex and shows a different behavior along the two slits. The velocity distribution along the slit with PA = 33° (i.e., along the long axis of the IR nebula) shows that the northeast rim of the optical shell is approaching us with a velocity of about 20–30 km s^{-1}, while the rim of the opposite side of the shell is receding from us with about the same velocity. This suggests that the outer parts of WS29 might be rotating around an axis aligned with the slit at PA = 120° (we discuss this possibility in Section 6.2). The velocity distribution along the slit with PA = 120° indicates that we see an expanding bilobal structure, whose existence also follows from the presence of filaments protruding in the southeast and northwest directions beyond the main (almost circular) optical shell (the origin of these protrusions is discussed in Section 6.2 as well).

Figure 13 shows the 1D low-resolution RSS spectrum of WS29 obtained by summing up, without any weighting, all rows from the area of an annulus with an outer radius of 40 arcsec centered on ALS 19653 and the central ±5 arcsec excluded. The emission lines (Hβ, Hα, and [N II] $\lambda\lambda$6548, 6584) detected in the resulting spectrum were measured using the programs described in Kniazev et al. (2004). Table 6 lists the observed intensities of these lines normalized to Hβ, $F(\lambda)/F({\rm H}\beta)$; the reddening-corrected line intensity ratios, $I(\lambda)/I({\rm H}\beta)$; and the logarithmic extinction coefficient, $C({\rm H}\beta)$, which corresponds to $E(B-V) = 1.94 \pm 0.56$ mag. This value of $E(B-V)$ agrees within the error margins with the color excess of ALS 19653 of $E(B-V) = 2.22 \pm 0.06$ mag based on the B and V magnitudes of this star (see Table 1) and the intrinsic color of a B0.5 Ib star of $(B-V)_0 = -0.22$ mag (Fitzgerald 1970).

6. Discussion

6.1. WS3 and BD+60° 2668A&B

The similar distances to and radial velocities of BD+60° 2668A&B, and the small angular (or projected linear) separation between these stars of ≈3 arcsec (or ≈0.05 pc) strongly suggest that they are members of the same stellar system. We note that both stars are located within the boundaries of the Cas OB5 association (Humphreys 1978) and that the *Gaia* DR2 parallaxes of a large part of stars listed in Humphreys (1978; see there Table 8) as the association members are similar to those of BD+60° 2668A&B. This implies that BD+60° 2668A&B reside in Cas OB5 and justifies why we adopt the same distance to both stars (see Section 2).

Using the adopted distance of 3.6 kpc, the B and V photometry from Table 1, $T_{\rm eff}$ from Table 3, $(B-V)_0$ colors and bolometric corrections from Fitzgerald (1970), and assuming that the total-to-selective absorption ratio equals 3.1, we calculate the absolute visual and bolometric magnitudes: $M_V \approx -5.4$ mag and $M_{\rm bol} \approx -7.9$ mag for BD+60° 2668A and $M_V \approx -4.6$ mag and $M_{\rm bol} \approx -6.8$ mag for BD+60° 2668B. The derived values of $M_{\rm bol}$ translate into bolometric luminosities of BD+60° 2668A&B of $\log(L/L_\odot) \approx 5.0$ and 4.6, which, along with the effective temperatures of these stars, imply that both of them are still on the main sequence or only recently left it, and that their initial (zero-age main-sequence) masses were, respectively, $M_{\rm ZAMS} \approx 20$ and $15\,M_\odot$ (e.g., Brott et al. 2011).

The inference that both BD+60° 2668A&B are relatively unevolved is supported by the surface elemental abundances measured for these stars. The comparison of the CNO

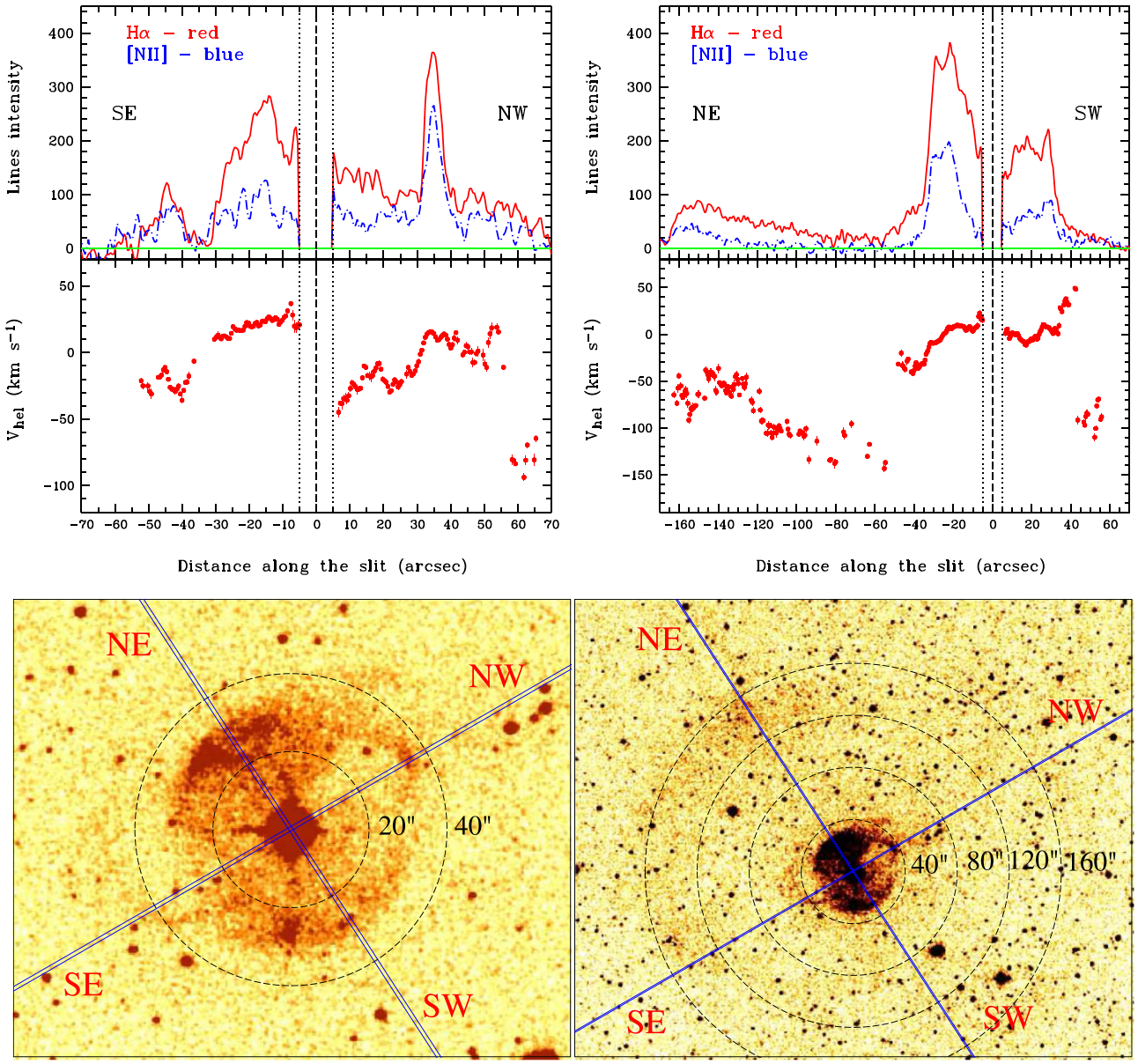

Figure 12. Upper panels: distributions of the Hα and [N II] λ6584 emission line intensities and Hα heliocentric radial velocity, V_{hel}, in the high-resolution RSS spectra of WS29 and its surroundings along the slits with PA = 120° (left-hand panel) and 33° (right-hand panel). The dashed vertical line in both panels corresponds to the position of ALS 19653, while the dotted vertical lines ±5 arcsec from the central line mark the area where the line intensities and velocity were not measured because of the effect of the star. The directions of the slits are shown. Bottom panels: IPHAS Hα images of WS29 and its surroundings with the slit positions shown by blue rectangles of angular width of 2 arcsec. Concentric, dashed circles are overplotted on the images to facilitate their comparison with the upper panels.

abundances of BD+60° 2668A given in Table 4 with those predicted for 20 $M_{\odot}$ rotating main-sequence stars by the stellar evolutionary models of Brott et al. (2011) shows that they agree with each other well enough if the initial rotational velocity of BD+60° 2668A was ~400 km s^{-1}, meaning that the enhanced nitrogen abundance of this star could be caused by rotational mixing. The only difference is that Brott et al.'s models predict a 0.2 dex lower O abundance, which could be due to the lower initial abundance for this element (as compared to the CAS) adopted in these models (see Table 4). Brott et al.'s models also suggest that the age of BD+60° 2668A is ≈7–8 Myr. Similarly, we found that the CNO abundances of BD+60° 2668B would reasonably agree with the model predictions if the initial rotational velocity of this star was ~200 km s^{-1}. The models also suggest that the age of BD+60° 2668B is ≈11 Myr, i.e., a factor of ≈1.5 higher than that of BD+60° 2668A.

The age estimates for BD+60° 2668A&B are in seeming contradiction with the possibility that the two stars are members of the same stellar system. The age discrepancy, however, could be understood if BD+60° 2668A is a blue straggler, i.e., a rejuvenated product of binary mass transfer or merger, implying that this star is or was a binary system. This possibility appears reasonable because the majority of massive stars are formed in binary and multiple systems and because their evolution is dominated by various binary-interaction processes (Sana et al. 2012). Moreover, the binary population synthesis modeling shows (de Mink et al. 2014) that about 30% of massive stars undergo binary interaction (i.e., mass transfer, common-envelope evolution, and/or merger) during the main-sequence stage.

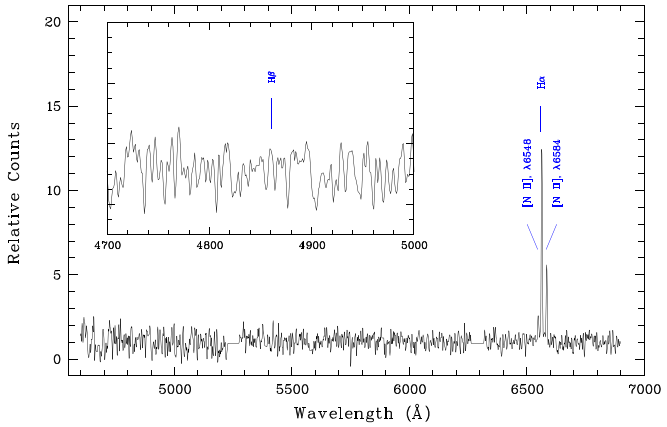

Figure 13. 1D low-resolution RSS spectrum of WS29. The insert shows a part of the spectrum around the Hβ line.

Table 6
Line Intensities in the Low-resolution RSS Spectrum of WS29

λ_0(Å) Ion	$F(\lambda)/F(\mathrm{H}\beta)$	$I(\lambda)/I(\mathrm{H}\beta)$
4861 Hβ	1.00 ± 0.61	1.00 ± 0.64
6548 [N II]	3.23 ± 2.33	0.37 ± 0.30
6563 Hα	26.17 ± 18.92	2.94 ± 2.13
6584 [N II]	10.33 ± 6.80	1.13 ± 0.85
$C(\mathrm{H}\beta)$	2.86 ± 0.82	
$E(B-V)$	1.94 ± 0.56 mag	

Enhancement of the nitrogen abundance by a factor of several on the surface of BD+60° 2668A could be the result of binary interaction as well (see Langer 2012).

Figure 1 shows that the circumstellar nebula around BD +60° 2668A&B is composed of two distinct components: a diffuse halo and an inner shell. Similar two-component nebulae were also detected around two candidate LBVs, GAL 079.29 + 00.46 (Gvaramadze et al. 2010b; see their Figure 2(j)) and [GKF2010] MN112 (Gvaramadze et al. 2010a; see their Figure 1). The morphology of these nebulae might be interpreted as indicating that their central stars experienced a brief episode of enhanced mass loss, leading to the formation of a compact region of dense material (visible in Hα as a density-bounded H II region—the halo), and that afterwards the stellar wind increases its speed and sweeps up the material of the preceding slower wind, and thereby creates a shell within the halo.

In the life of a single massive star, such changes in the mass-loss rate and wind velocity can occur if after the red supergiant stage the star becomes a Wolf-Rayet star or undergoes a blue loop evolution. The CNO abundances derived for BD+60° 2668A&B, however, suggest that these stars have not yet gone through the red supergiant stage. Besides this, the episode of enhanced mass loss and subsequent increase of the wind velocity could be caused by the bi-stability jump (Pauldrach & Puls 1990; Lamers & Pauldrach 1991) if in the course of stellar evolution the effective temperature falls below some critical value (≈21–22 kK) and then again increases above it. According to the stellar evolutionary models by Brott et al. (2011), for 15–20 $M_\odot$ stars, this situation takes place during the transition from core-H to core-He burning. The duration of this transition of $\sim 10^5$ years, however, is too long, and the wind velocity is too high ($\sim$1000 km s^{-1}) to result in a compact (parsec-size) circumstellar nebula.

On the other hand, as discussed above, BD+60° 2668A might be the result of a merger of two stars, which causes a temporary inflation of the resulting single star and a decrease of its $T_{\rm eff}$ below the temperature of the bi-stability jump. As a result of this, the stellar wind velocity drops by a factor of 2, while the mass-loss rate increases by a factor of 10 (Vink 2018), leading to a factor of 20 increase of the stellar wind density and formation of a halo around the star. Later on, after the thermal adjustment of the merger product on its Kelvin–Helmholtz timescale ($\sim 10^4$ years), the effective temperature of the star increases above the temperature of the bi-stability jump, and the stellar wind velocity increases to its initial value, which in turn leads to the formation of a shell within the halo. Since the (relaxed) merger product is expected to be a fast-rotating star, the temperature distribution across its surface could be inhomogeneous due to gravity-darkening. Correspondingly, the wind velocity along the stellar rotational axis might be higher than in the equatorial region, which could be responsible for the observed elongated shape of the shell (see Figure 1). We speculate also that the postmerger relaxation of the newly formed single star might be accompanied by photometric and spectroscopic variability typical of LBVs and that in the recent past BD+60° 2668A probably looked like an LBV.

The possibility that LBV activity (including giant, η Car-like, eruptions) is triggered by the interaction between companion stars in binary or triple systems (e.g., through the merger of two stars, tidal interaction, or interchange of components) has been widely discussed in the last two decades (e.g., Justham et al. 2014; Portegies Zwart & van den Heuvel 2016 and references therein). Since this interaction can take place at both early and late stages of evolution of binary/triple systems, it is natural to expect that the LBV phenomenon (accompanied by the formation of circumstellar nebulae) can be found among massive stars at both early and advanced evolutionary stages. It should also be noted that the detection of possible companion stars in wide orbits around several (candidate) LBVs (e.g., Martayan et al. 2016) does not contradict the possibility that the LBV activity of these stars is caused by binary-interaction processes. In such cases, the (candidate) LBV stars might be unresolved binaries or the merger products of two stars, while the nearby stars might represent the tertiary stars dynamically scattered in wide orbits (see Reipurth & Mikkola 2012) or former (unbound) members of dissolved triple systems (see Gvaramadze & Menten 2012). BD+60° 2668B might be such a tertiary star.

In summary, the spectral analysis of BD+60° 2668A&B indicates that both stars are either still on the main sequence or only recently left it, and that the surface nitrogen abundance of BD+60° 2668A is enhanced by a factor of several. Also, it appears that BD+60° 2668A is a factor of two younger than BD+60° 2668B despite strong indications that both stars are members of the same stellar system and, therefore, most likely were formed simultaneously. The age discrepancy could be naturally understood if BD+60° 2668A is a rejuvenated product of binary interaction, in which case the enhanced nitrogen abundance on the surface of the star is a direct consequence of this interaction. The binary-interaction scenario also provides a framework for understanding the origin of circumstellar nebula, which can hardly be produced by a single unevolved star.

6.2. WS29 and ALS 19653

For ALS 19653, we derive $M_V \approx -5.5$ mag and $\log(L/L_\odot) \approx 5.1$, which, along with the effective temperature, imply an initial mass and age of ALS 19653 of, respectively, $\approx 20\,M_\odot$ and ≈7–8 Myr, meaning that this star is either still on the main sequence or has just left it (e.g., Brott et al. 2011).

The chemical abundances derived for ALS 19653 (see Table 4) support the inference that this star is relatively unevolved and agree with Brott et al.'s models if the initial rotational velocity of this star was $\sim 200\,\mathrm{km\,s^{-1}}$. Note that the uncertainties in the measurements allow the possibility that the surface nitrogen abundance is enhanced by factors of 2 or 3 in comparison with the CAS or the initial nitrogen abundance adopted in Brott et al. (2011), respectively. This enhancement, if real, could be caused not only by rotationally induced mixing, but also by binary interaction, e.g., because of accretion of CNO-processed material from the companion star or mixing caused by the merger of the binary components (e.g., Langer 2012).

The detection of two nested shells around ALS 19653 indicates that this star has experienced at least two episodes of enhanced mass loss.[11] At the adopted distance to ALS 19653, the characteristic radius of the second (outer) shell is ≈1.2 pc, which along with the expansion velocity of this shell of $\sim 100\,\mathrm{km\,s^{-1}}$ gives its kinematic age of $\sim 10^4$ years. Similarly, assuming that the optical shell of WS29 is expanding with a velocity of 20–30 $\mathrm{km\,s^{-1}}$ (see Figure 12) and given its characteristic radius of ≈0.2 pc, one finds that this shell was formed shortly after the outer shell. WS29 is especially curious because it consists of an optical circular shell with protrusions in the northwest and southeast directions, and an inner elongated IR nebula, stretched in the direction perpendicular to the axis defined by the protrusions. Below we discuss the possible origin of WS29.

The changes in the Hα line profile suggest that ALS 19653 is surrounded by a disk-like structure viewed nearly edge-on (see Section 4.2), while the polarization angle of the stellar light of 121° (see Section 2) implies that this structure is oriented in the same direction as the IR nebula. We therefore interpret this nebula as a flattened outflow or ejecta from ALS 19653 viewed nearly edge-on. Since it is unlikely that a single unevolved star can produce a circumstellar nebula, it is reasonable to assume that its formation is due to a binary-interaction process, e.g., because of the merger of two stars or common-envelope evolution. Correspondingly, the spin axis of the merger product or the angular momentum of the post-common-envelope binary orbit should coincide with the line connecting the protrusions in the optical shell of WS29 (PA ≈ 120°). If ALS 19653 is indeed the result of merger of two stars, then the inclination angle of its rotational axis to our line of sight should be close to 90°, while its equatorial rotational velocity should be almost equal to the projected rotational velocity of $28\,\mathrm{km\,s^{-1}}$. The Hα line variability in ALS 19653 could be understood if the density structure of the (inner part of the) flattened circumstellar nebula is non-axisymmetric, e.g., because of the tidal force from the companion star (see Okazaki et al. 2002; Oktariani & Okazaki 2009). The possible binary nature of ALS 19653 (see Section 4.2) makes this explanation plausible. It should be noted, however, that the binarity of ALS 19653 does not exclude the possibility that this star is a merger product because originally it might have been a triple system (see Pasquali et al. 2000; Schneider et al. 2016).

The strong differential rotation originating in the course of the merger of a binary system or common-envelope evolution might be responsible for the generation of a strong large-scale magnetic field in the newly formed single star (Langer 2012; Wickramasinghe et al. 2014; Schneider et al. 2016) or in the ejected envelope (Regös & Tout 1995; Tout & Regós 2003), respectively. This magnetic field can in turn effectively spin down the merger product through dynamical mass loss (e.g., Langer 2012) and may affect (or even determine) the geometry of the ejected material (Chevalier & Luo 1994; Różyczka & Franco 1996; Garcia-Segura et al. 1999; Nordhaus & Blackman 2006). Correspondingly, the low rotational velocity derived for ALS 19653 might be the direct result of magnetic braking of this star, while the origin of protrusions in the northwest and southeast directions might be caused by the deflection of ejected material toward the polar directions by the tension of the toroidal magnetic field. The gravity-darkening of the initially fast-rotating merger remnant may also contribute to the origin of the polar protrusions.

Finally, we note that the distribution of the Hα radial velocity along the slit with PA = 33° (i.e., along the slit aligned with the IR nebula) suggests that the outer parts of the equatorial ejecta might be rotating around the axis defined by the orientation of the polar protrusions. If real, this rotation would imply a very efficient transfer of angular momentum from the merger remnant (possibly rotating at break-up velocity at the equator) or from the shrinking binary system to a tiny fraction of the equatorial ejecta by means of magnetic torque. A follow-up study of the Hα velocity field in WS29 with the Multi-Unit Spectroscopic Explorer (MUSE; Bacon et al. 2010) could potentially clarify this issue.

7. Summary

We discovered two mid-infrared nebulae using data from the *WISE* survey and identified their central stars with the early B stars BD+60° 2668 and ALS 19653. Our spectroscopic observations of BD+60° 2668 (composed of two components, A and B, separated by ≈3 arcsec) and ALS 19653 confirmed that they are massive stars. We analyzed spectra of these stars with the stellar atmosphere code FASTWIND and found that all three stars are either on the main sequence or have just left it. The obtained results provide further support to claims that massive stars can produce circumstellar nebulae during the early stages of evolution. Since the origin of such nebulae can hardly be understood within the framework of single-star evolution, and because the majority of massive stars form in binary or multiple systems and many of them undergo binary interaction during the main-sequence stage, we suggested that the formation of both nebulae is related to the binary nature of their central stars. We found that the surface nitrogen abundance of BD+60° 2668A is enhanced by a factor of several with respect to the solar value and that the apparent age of this star is a factor of 1.5 younger than that of BD+60° 2668B. Proceeding from this, we suggested that component A is a rejuvenated product of a binary merger and that the mass loss from just this star is responsible for the origin of the nebula around BD+60° 2668. We also found that ALS 19653 shows

[11] A similar two-shell structure was also found around the O6.5f?p (Walborn et al. 2010) star HD 148937 (Leitherer & Chavarria-K 1987). It is believed that the strong magnetic field of this star, its rapid rotation, and the origin of the nitrogen-rich circumstellar nebula are the result of the merger of two stars (Langer 2012).

significant radial velocity variations, meaning that it is a close binary system. This and the presence of a disk-like structure around ALS 19653 (as suggested by polarimetric, infrared, and radio observations, and the variable profile of the Hα emission line in the spectrum of this star) suggest that the associated nebula might also be caused by binary interaction.

This work is based on observations collected with the Southern African Large Telescope (SALT), programmes 2016-1-SCI-012 and 2017-1-SCI-006, and at the Centro Astronómico Hispano Alemán (CAHA), operated jointly by the Max-Planck Institut für Astronomie and the Instituto de Astrofisica de Andalucia (CSIC), programme H12-3.5-013, and supported by the Russian Foundation for Basic Research grant 16-02-00148. A.Y.K. acknowledges support from the National Research Foundation (NRF) of South Africa. E.K.G. gratefully acknowledges funding by the Sonderforschungsbereich "The Milky Way System" (SFB 881, especially subproject A5) of the German Research Foundation (DFG). This work has made use of data products from the *Wide-field Infrared Survey Explorer*, which is a joint project of the University of California, Los Angeles, and the Jet Propulsion Laboratory/California Institute of Technology, funded by the National Aeronautics and Space Administration, the SIMBAD database and the VizieR catalog access tool, both operated at CDS, Strasbourg, France. This work has also made use of data from the European Space Agency (ESA) mission *Gaia* (https://www.cosmos.esa.int/gaia), processed by the *Gaia* Data Processing and Analysis Consortium (DPAC https://www.cosmos.esa.int/web/gaia/dpac/consortium). Funding for the DPAC has been provided by national institutions, in particular the institutions participating in the *Gaia* Multilateral Agreement.

Software: FASTWIND (Santolaya-Rey et al. 1997; Puls et al. 2005; Rivero González et al. 2012), IRAF (Tody 1986, 1993), IACOB-BROAD (Simón-Diaz & Herrero 2007, 2014), ULYSS (Koleva et al. 2009).

ORCID iDs

Vasilii V. Gvaramadze https://orcid.org/0000-0003-1536-8417
Alexei Yu. Kniazev https://orcid.org/0000-0001-8646-0419
Norberto Castro https://orcid.org/0000-0003-0521-473X

References

Bacon, R., Accardo, M., Adjali, L., et al. 2010, Proc. SPIE, 7735, 773508
Balona, L., & Crampton, D. 1974, MNRAS, 166, 203
Barnes, S. I., Cottrell, P. L., Albrow, M. D., et al. 2008, Proc. SPIE, 7014, 70140K
Bohlin, R. C. 1996, AJ, 111, 1743
Bramall, D. G., Schmoll, J., Tyas, L. M. G., et al. 2012, Proc. SPIE, 8446, 84460A
Bramall, D. G., Sharples, R., Tyas, L., et al. 2010, Proc. SPIE, 7735, 77354F
Brighenti, F., & D'Ercole, A. 1995, MNRAS, 277, 53
Brodskaya, E. S. 1953, IzKrY, 10, 104
Brott, I., de Mink, S. E., Cantiello, M., et al. 2011, A&A, 530, A115
Buckley, D. A. H., Swart, G. P., & Meiring, J. G. 2006, Proc. SPIE, 6267, 62670Z
Burgh, E. B., Nordsieck, K. H., Kobulnicky, H. A., et al. 2003, Proc. SPIE, 4841, 1463
Castro, N., Urbaneja, M. A., Herrero, A., et al. 2012, A&A, 542, A79
Chevalier, R. A., & Luo, D. 1994, ApJ, 421, 225
Chini, R., Hoffmeister, V. H., Nasseri, A., Stahl, O., & Zinnecker, H. 2012, MNRAS, 424, 1925
Clark, J. S., Larionov, V. M., & Arkharov, A. 2005, A&A, 435, 239
Condon, J. J., Cotton, W. D., Greisen, E. W., et al. 1998, AJ, 115, 1693
Condon, J. J., Kaplan, D. L., & Terzian, Y. 1999, ApJS, 123, 219
Corradi, R. L. M., & Schwarz, H. E. 1993, A&A, 268, 714
Crause, L. A., Sharples, R. M., Bramall, D. G., et al. 2014, Proc. SPIE, 9147, 91476T
Crawford, S. M., Still, M., Schellart, P., et al. 2010, Proc. SPIE, 7737, 773725
De Marco, O. 2009, PASP, 121, 316
de Mink, S. E., Sana, H., Langer, N., Izzard, R. G., & Schneider, F. R. N. 2014, ApJ, 782, 7
Douglass, G. G., Mason, B. D., Germain, M. E., & Worley, C. E. 1999, AJ, 118, 1395
Drew, J., Greimel, R., Irwin, M. J., et al. 2005, MNRAS, 362, 753
Evans, C. J., Howarth, I. D., Irwin, M. J., Burnley, A. W., & Harries, T. J. 2004, MNRAS, 353, 601
Fabian, A. C., & Hansen, C. J. 1979, MNRAS, 187, 283
Fitzgerald, M. P. 1970, A&A, 4, 234
Flagey, N., Noriega-Crespo, A., Petric, A. O., & Geballe, T. R. 2014, AJ, 148, 34
Fullerton, A. W., Massa, D. L., Prinja, R. K., Owocki, S. P., & Cranmer, S. R. 1997, A&A, 327, 699
Gaia Collaboration, Brown, A. G. A., Vallenari, A., et al. 2018, A&A, 616, A1
Garcia-Segura, G., Langer, N., & Mac Low, M.-M. 1996, A&A, 316, 133
Garcia-Segura, G., Langer, N., Różyczka, M., & Franco, J. 1999, ApJ, 517, 767
Gvaramadze, V. V., & Kniazev, A. Y. 2017, in ASP Conf. Ser. 508, The B[e] Phenomenon. Forty Years of Studies, ed. A. S. Miroshnichenko et al. (San Francisco, CA: ASP), 207
Gvaramadze, V. V., Kniazev, A. Y., Fabrika, S., et al. 2010a, MNRAS, 405, 520
Gvaramadze, V. V., Kniazev, A. Y., & Fabrika, S. 2010b, MNRAS, 405, 1047
Gvaramadze, V. V., Kniazev, A. Y., Maryeva, O. V., & Berdnikov, L. N. 2018, MNRAS, 474, 1412
Gvaramadze, V. V., & Menten, K. M. 2012, A&A, 541, A7
Gvaramadze, V. V., Miroshnichenko, A. S., Castro, N., Langer, N., & Zharikov, S. V. 2014, MNRAS, 437, 2761
Gvaramadze, V. V., Fabrika, S., Hamann, W.-R., et al. 2009, MNRAS, 400, 524
Gvaramadze, V. V., Kniazev, A. Y., Bestenlehner, J. M., et al. 2015, MNRAS, 454, 219
Gvaramadze, V. V., Kniazev, A. Y., Miroshnichenko, A. S., et al. 2012, MNRAS, 421, 3325
Henden, A. A., Templeton, M., Smith, T. C., Levine, S., & Welch, D. 2016, yCat, 2336, 0
Hendry, M. A., Smartt, S. J., Skillman, E. D., et al. 2008, MNRAS, 388, 1127
Humphreys, R. M. 1978, ApJS, 38, 309
Humphreys, R. M., & Davidson, K. 1994, PASP, 106, 1025
Humphreys, R. M., & McElroy, D. B. 1984, ApJ, 284, 565
Justham, S., Podsiadlowski, P., & Vink, J. S. 2014, ApJ, 796, 121
Kaufer, A., Stahl, O., Wolf, B., et al. 1996, A&A, 305, 887
Kharchenko, N. V. 2001, KFNT, 17, 409
Kniazev, A. Y., & Gvaramadze, V. V. 2015, in Proc. SALT Science Conf. 2015 (SSC2015), ed. D. Buckley & A. Schroeder (South Africa: Stellenbosch Institute of Advanced Study), 49
Kniazev, A. Y., Gvaramadze, V. V., & Berdnikov, L. N. 2015, MNRAS, 449, L60
Kniazev, A. Y., Gvaramadze, V. V., & Berdnikov, L. N. 2016, MNRAS, 459, 3068
Kniazev, A. Y., Pustilnik, S. A., Grebel, E. K., Lee, H., & Pramskij, A. G. 2004, ApJS, 153, 429
Kniazev, A. Y., Zijlstra, A. A., Grebel, E. K., et al. 2008, MNRAS, 388, 1667
Kobulnicky, H. A., Nordsieck, K. H., Burgh, E. B., et al. 2003, Proc. SPIE, 4841, 1634
Koleva, M., Prugniel, P., Bouchard, A., & Wu, Y. 2009, A&A, 501, 1269
Kronberger, M., Parker, Q. A., Jacoby, G. H., et al. 2016, JPhCS, 728, 072012
Kudritzki, R.-P., & Puls, J. 2000, ARA&A, 38, 613
Lamers, H. J. G. L. M., Nota, A., Panagia, N., Smith, L. J., & Langer, N. 2001, ApJ, 551, 764
Lamers, H. J. G. L. M., & Pauldrach, A. W. A. 1991, A&A, 244, L5
Lamers, H. J. G. L. M., Snow, T. P., & Lindholm, D. M. 1995, ApJ, 455, 269
Langer, N. 1998, A&A, 329, 551
Langer, N. 2012, ARA&A, 50, 107
Lefever, K., Puls, J., Morel, T., et al. 2010, A&A, 515, A74
Leitherer, C., & Chavarria-K, C. 1987, A&A, 175, 208
Livio, M., Salzman, J., & Shaviv, G. 1979, MNRAS, 188, 1
Mackey, J., Mohamed, S., Gvaramadze, V. V., et al. 2014, Natur, 512, 282

Mahy, L., Hutsemékers, D., Royer, P., & Waelkens, C. 2016, A&A, 594, A94
Markova, N., & Valchev, T. 2000, A&A, 363, 995
Martayan, C., Lobel, A., Baade, D., et al. 2016, A&A, 587, A115
Mastrodemos, N., & Morris, M. 1999, ApJ, 523, 357
McLean, B. J., Greene, G. R., Lattanzi, M. G., & Pirenne, B. 2000, in ASP Conf. Ser. 216, Astronomical Data Analysis Software and Systems IX, ed. N. Manset, C. Veillet, & D. Crabtree (San Francisco, CA: ASP), 145
Mizuno, D. R., Kraemer, K. E., Flagey, N., et al. 2010, AJ, 139, 1542
Morgan, W. W., Code, A. D., & Whitford, A. E. 1955, ApJS, 2, 41
Morris, M. 1981, ApJ, 249, 572
Morris, M., & Jura, M. 1983, ApJ, 267, 179
Nassau, J. J., & Morgan, W. W. 1951, ApJ, 113, 141
Nieva, M.-F., & Przybilla, N. 2012, A&A, 539, A143
Nordhaus, J., & Blackman, E. G. 2006, MNRAS, 370, 2004
Nota, A., Livio, M., Clampin, M., & Schulte-Ladbeck, R. 1995, ApJ, 448, 788
O'Donoghue, D., Buckley, D. A. H., Balona, L. A., et al. 2006, MNRAS, 372, 151
Okazaki, A. T., Bate, M. R., Ogilvie, G. I., & Pringle, J. E. 2002, MNRAS, 337, 967
Oktariani, F., & Okazaki, A. T. 2009, PASJ, 61, 57
Parker, Q. A., Bojičić, I. S., & Frew, D. J. 2016, JPhCS, 728, 032008
Pasquali, A., Nota, A., Langer, N., Schulte-Ladbeck, R. E., & Clampin, M. 2000, AJ, 119, 1352
Pauldrach, A. W. A., & Puls, J. 1990, A&A, 237, 409
Petrenz, P., & Puls, J. 1996, A&A, 312, 195
Portegies Zwart, S. F., & van den Heuvel, E. P. J. 2016, MNRAS, 456, 3401
Prugniel, P., Vauglin, I., & Koleva, M. 2011, A&A, 531, 165
Puls, J., Urbaneja, M. A., Venero, R., et al. 2005, A&A, 435, 669
Radoslavova, T. 1989, ABaOB, 66, 33
Regös, E., & Tout, C. A. 1995, MNRAS, 273, 146
Reipurth, B., & Mikkola, S. 2012, Natur, 492, 221
Rivero González, J. G., Puls, J., Massey, P., & Najarro, F. 2012, A&A, 543, A95
Różyczka, M., & Franco, J. 1996, ApJL, 469, L127
Rodrigues, C. V., Sartori, M. J., Gregorio-Hetem, J., & Magalhães, A. M. 2009, ApJ, 698, 2031
Sana, H., de Mink, S. E., de Koter, A., et al. 2012, Sci, 337, 444
Santolaya-Rey, A. E., Puls, J., & Herrero, A. 1997, A&A, 323, 488
Schneider, F. R. N., Podsiadlowski, P., Langer, N., Castro, N., & Fossati, L. 2016, MNRAS, 457, 2355
Silva, K. M., Flagey, N., Noriega-Crespo, A., Carey, S., & Ingallinera, A. 2017, AJ, 153, 115
Simón-Diaz, S., & Herrero, A. 2007, A&A, 468, 1063
Simón-Diaz, S., & Herrero, A. 2014, A&A, 562, A135
Skrutskie, M. F., Cutri, R. M., Stiening, R., et al. 2006, AJ, 131, 1163
Smartt, S. J., Lennon, D. J., Kudritzki, R. P., et al. 2002, A&A, 391, 979
Smith, N., Arnett, W. D., Bally, J., Ginsburg, A., & Filippenko, A. V. 2013, MNRAS, 429, 1324
Stringfellow, G. S., Gvaramadze, V. V., Beletsky, Y., & Kniazev, A. Y. 2012a, Proc. IAU Symp. 282, From Interacting Binaries to Exoplanets: Essential Modelling Tools, ed. M. T. Richards & I. I. Hubeny (Cambridge: Cambridge Univ. Press), 267
Stringfellow, G. S., Gvaramadze, V. V., Beletsky, Y., & Kniazev, A. Y. 2012b, ASP Conf. Ser. 465, Four Decades of Massive Star Research—A Scientific Meeting in Honor of Anthony J. Moffat, ed. L. Drissen et al. (San Francisco, CA: ASP), 514
Tody, D. 1986, Proc. SPIE, 627, 733
Tody, D. 1993, in ASP Conf. Ser. 52, Astronomical Data Analysis Software and Systems II, ed. R. J. Hanisch, R. J. V. Brissenden, & J. Barnes (San Francisco, CA: ASP), 173
Tout, C. A., & Regős, E. 2003, in ASP Conf. Ser. 293, 3D Stellar Evolution, ed. S. Turcotte, S. C. Keller, & R. M. Cavallo (San Francisco, CA: ASP), 100
Verdugo, E., Talavera, A., & Gómez de Castro, A. I. 2000, in ASP Conf. Ser. 214, The Be Phenomenon in Early-Type Stars, ed. M. A. Smith & H. F. Henrichs (San Francisco, CA: ASP), 91
Vieira, S. L. A., Corradi, W. J. B., Alencar, S. H. P., et al. 2003, AJ, 126, 2971
Vink, J. S. 2018, A&A, 619, A54
Wachter, S., Mauerhan, J. C., van Dyk, S. D., et al. 2010, AJ, 139, 2330
Walborn, N. R., & Fitzpatrick, E. L. 1990, PASP, 102, 379
Walborn, N. R., Sota, A., Maiz Apellániz, J., et al. 2010, ApJL, 711, L143
Wickramasinghe, D. T., Tout, C. A., & Ferrario, L. 2014, MNRAS, 437, 675
Wright, E. L., Eisenhardt, P. R. M., Mainzer, A. K., et al. 2010, AJ, 140, 1868